Highlights

- Neural trajectories in the hippocampus exhibited greater variability during a working memory (WM) task compared to those in the entorhinal cortex and amygdala regions.

- The distance of neural trajectories between encoding and retrieval states in the hippocampus was memory-load dependent during a WM task.

- Hippocampal neural trajectories fluctuated between the encoding and retrieval states in a task-dependent manner during both baseline and sharp-wave ripple (SWR) periods.

- Hippocampal neural trajectories shifted from encoding to retrieval states during SWR period.

Hippocampal neural fluctuations between memory encoding and retrieval states during a working memory task in humans

Yusuke Watanabe[a,*], Yuji Ikegaya[b,c,d], Takufumi Yanagisawa[a,e]

[a]*Institute for Advanced Cocreation studies, Osaka University, 2-2 Yamadaoka, Suita, 565-0871, Osaka, Japan*
[b]*Graduate School of Pharmaceutical Sciences, The University of Tokyo, 7-3-1 Hongo, Tokyo, 113-0033, Japan*
[c]*Institute for AI and Beyond, The University of Tokyo, 7-3-1 Hongo, Tokyo, 113-0033, Japan*
[d]*Center for Information and Neural Networks, National Institute of Information and Communications Technology, 1-4 Yamadaoka, Suita City, 565-0871, Osaka, Japan*
[e]*Department of Neurosurgery, Osaka University Graduate School of Medicine, 2-2 Yamadaoka, Osaka, 565-0871, Japan*

Abstract

Working memory (WM) serves as a critical cornerstone in a multitude of cognitive functions; yet, the elaborate neural mechanisms underpinning its functionality remain incompletely understood. Specifically, while both the hippocampus and sharp-wave ripple complexes (SWRs) — rapid, coordinated neural occurrences within the hippocampus — are recognized for their roles in memory consolidation and retrieval, their involvement in WM tasks persists as somewhat equivocal. Our present research theorizes that the multiunit activity patterns within the hippocampus work synergistically with SWRs, thereby demonstrating distinctive dynamism during WM tasks. Our investigation involved an in-depth analysis of a dataset derived from intracranial electroencephalogram recordings acquired from the medial temporal lobe (MTL) of nine individuals with epilepsy performing an eight-second Sternberg task. We employed Gaussian-process factor analysis to discern low-dimensional neural representations, or 'trajectories,' within the MTL territories during the WM task. Our findings revealed that the neural trajectory exhibited the most significant variations in the hippocampus when compared to the entorhinal cortex and amygdala. Moreover, divergence in the trajectories identified between encoding and retrieval phases were memory load-dependent. Importantly, hippocampal trajectories oscillated during the retrieval phase, displaying task-dependent transitions between encoding and retrieval states, inclusive of baseline and SWR episodes. These oscillations shifted from encoding to retrieval states in accordance with SWRs. Hence, these results highlight the critical role of the hippocampus in performing WM tasks and propose a persuasive hypothesis for subsequent investigation: the functional state of the hippocampus transitions from encoding to retrieval during SWRs.

Keywords: working memory, WM, memory load, hippocampus, sharp-wave ripples, SWR, humans

1. Introduction

Working memory (WM) plays a crucial role in everyday life, and its neural underpinnings remain an area of ongoing research. The hippocampus, notably integral to memory, continues to be a primary focus of this investigation [1] [2] [3] [4] [5] [6] [7] [8] [9]. Gaining insights into the role of the hippocampus in working memory is vital to deepening our understanding of cognitive processes, hence fostering the progression of cognitive training and interventions.

Current evidence suggests a transient, synchronized oscillation, referred to as sharp-wave ripple (SWR) [10], is linked with several cognitive functions, such as memory replay [11] [12] [13] [14] [15], memory consolidation [16] [17] [18] [19], memory recall [20] [21] [22], and neural plasticity [23] [24]. This evidence indicates the likelihood that SWR could be a critical component of hippocampal processing, contributing to working memory performance. However, research investigating the effects of SWRs on working memory remains sparse [25], and is largely limited to rodent models par-

*Corresponding author. Tel: +81-6-6879-3652

ticipating in navigation tasks where the timing of memory acquisition and recall is not explicitly distinguished.

Recent studies indicate that hippocampal neurons exhibit low-dimensional representations during WM tasks. Notably, the firing patterns of place cells [26] [27] [28] [29] [30], located in the hippocampus, are observed to be encompassed within a dynamic, nonlinear three-dimensional hyperbolic geometry in rodents [31]. Moreover, grid cells in the entorhinal cortex (EC)—the dominant pathway to the hippocampus [32] [33] [34]—displayed toroidal topology during exploration [35]. Unfortunately, these investigations are confined to spatial navigation tasks in rodents, thus imposing limitations on the temporal resolution of WM tasks. The applicability of these findings to human subjects and their generalization beyond navigation tasks remains to be established.

Given these considerations, the current study aims to validate the hypothesis that hippocampal neurons exhibit distinctive representations in low-dimensional spaces, designated as 'neural trajectory,' during WM tasks, most prominently within SWR periods. To evaluate this claim, we employed a dataset of patients performing an eight-second Sternberg task with high temporal resolution (1 s for fixation, 2 s for encoding, 3 s for maintenance, and 2 s for retrieval), while their intracranial electroencephalography signals (iEEG) within the medial temporal lobe (MTL) were being monitored [36]. To investigate low-dimensional neural trajectories, we employed Gaussian-process factor analysis (GPFA), a method renowned for analyzing neural population dynamics [37].

2. Methods

2.1. Dataset

A publicly available dataset [36] was used, which consists of nine epilepsy patients performing a modified Sternberg task. This task involves four phases: fixation (1s), encoding (2s), maintenance (3s), and retrieval (2s) [36]. During the encoding phase, participants were exposed to four, six, or eight alphabet letters, referred to as the set size. Subsequently, they had to decide whether a probe letter presented during the retrieval phase was previously displayed (the correct choice for the Match IN task) or not (the correct choice for the Mismatch OUT task). iEEG signals were recorded at a sampling rate of 32 kHz, within a frequency range of 0.5–5,000 Hz, using depth electrodes implanted in the medial temporal lobe (MTL) regions: the anterior head of the left and the right hippocampus (AHL and AHR), the posterior body of the hippocampus (PHL and PHR), the entorhinal cortex (ECL and ECR), and the amygdala (AL and AR), as illustrated in Figure 1A and Table 1. The iEEG signals were subsequently downsampled to a rate of 2 kHz. Correlations among variables such as set size and correct rate were investigated (Figure **??**S1). The timings of multiunit spikes were determined by a spike sorting algorithm [38] using the Combinato package (`https://github.com/jniediek/combinato`)(Figure 1C).

2.2. Calculation of neural trajectories using GPFA

Neural trajectories, also termed 'factors' (Figure 1D), in the hippocampus, EC, and amygdala (Figure 1D), were computed using GPFA [37] applied to the multiunit activity data for each session. GPFA was performed with the elephant package (`https://elephant.readthedocs.io/en/latest/reference/gpfa.html`). The bin size was set to 50 ms, with no overlaps. Each factor was z-normalized across all sessions. The Euclidean distance from the origin (O) was then calculated (Figure 1E).

For each trajectory within a region, for instance, AHL, *geometric medians* (i.e., g_F for fixation, g_E for encoding, g_M for maintenance, and g_R for retrieval phase) were determined by calculating the median coordinates of the trajectory during the four phases (Figure 1D). An optimal dimensionality for GPFA was identified as three using the elbow method, which was derived by investigating the log-likelihood values through a three-fold cross-validation approach (Figure 2B).

2.3. Identifying SWR candidates from hippocampal regions

Potential SWR events within the hippocampus were detected using a widely accepted method [39]. LFP signals from a region of interest (ROI), such as AHL, were re-referenced by subtracting an averaged signal from locations outside the ROI (*e.g.*, AHR, PHL, PHR, ECL, ECR, AL, and AR) (see Figure 1A). The re-referenced LFP signals were then filtered with a ripple-band filter (80–140 Hz) to identify SWR candidates (=SWR^+

candidates) (see Figure 1B). SWR detection was conducted using a published tool (`https://github.com/Eden-Kramer-Lab/ripple_detection`) [40], with the bandpass range adjusted to 80–140 Hz for humans [21] [22], different from the original 150–250 Hz range typically applied to rodents.

Control events for SWR^+ candidates, labeled as SWR^- candidates, were identified by randomly shuffling the timestamps of SWR^+ candidates across all trials and subjects. The resulting SWR^+/SWR^- candidates were then subjected to visual inspection, as shown in Figure 1.

2.4. Defining SWRs from putative hippocampal CA1 regions

SWRs were distinguished from SWR candidates in presumptive CA1 regions. Initially, these regions were defined as follows: SWR^+/SWR^- candidates in the hippocampus were projected into a two-dimensional space based on overlapping spike counts per unit employing a supervised method using UMAP (Uniform Manifold Approximation and Projection) [41] (Figure 4A). Clustering validation was performed by computing the silhouette score [42] from clustered samples (Table 2). Regions in the hippocampus, which scored above 0.6 on average across sessions (75th percentile) (Figure 4B), were characterized as presumed CA1 regions, identifying five electrode positions from five patients (Table 3).

SWR^+/SWR^- candidates in the assumed CA1 regions were classified as SWR^+/SWR^-, thus relinquishing their candidate status. The duration and ripple band peak amplitude of SWRs were observed to follow log-normal distributions (Figure 44C & E). Each time period of SWR was partitioned relative to the time from the SWR center into pre- (at −800 to −300 ms from SWR center), mid- (at −250 to +250 ms), and post-SWR (at +300 to +800 ms) times.

2.5. Statistical evaluation

The Brunner–Munzel test and the Kruskal-Wallis test were performed using the SciPy package in Python [43]. Correlational analysis was performed by determining the rank of the observed correlation coefficient in its associated set-size-shuffled surrogate using a custom Python script. The bootstrap test was implemented using an in-house Python script.

3. Results

3.1. iEEG recording and neural trajectory in MTL regions during a Sternberg task

We leveraged a publicly available dataset for this analysis [36]. This dataset encompasses LFP signals (Figure 1A) from MTL regions (Table 1) during a modified Sternberg task execution. We identified SWR^+ candidates from LFP signals filtered through the 80–140 Hz ripple band (Figure 1B), originating across all hippocampal regions (refer to Methods). Correspondingly, SWR^- candidates were defined at identical timestamps) but shuffled across different trials (Figure 1). The dataset included multiunit spikes (Figure 1C) identified via a spike sorting algorithm [38]. By employing GPFA [37], and using the 50-ms binned multiunit activity with no overlaps, we determined the neural trajectories (or factors) of MTL regions by session and region (Figure 1D). We normalized each factor by session and region for instance, session #2 in AHL of subject #1. Subsequently, we calculated the Euclidean distance from the origin (O) (Figure 1E).

3.2. Hippocampal neural trajectory correlation with a Sternberg task

Figure 2A illustrates the cloud of median neural trajectories of 50 trials within the three main factor spaces. We determined the optimal embedding dimension for the GPFA model to be three, using the elbow method (Figure 2B). The trajectory distance from the origin (O) (represented as $\|g_F\|$, $\|g_E\|$, $\|g_M\|$, and $\|g_R\|$) in the hippocampus exceeded corresponding distances in the EC and amygdala (Figures 2C and D).[1]

Similarly, we computed the distances between the geometric medians of four phases, namely $\|g_F g_E\|$, $\|g_F g_M\|$, $\|g_F g_R\|$, $\|g_E g_M\|$, $\|g_E g_R\|$, and $\|g_M g_R\|$. The results indicated that the hippocampus displayed larger distances between phases than both the EC and amygdala. [2]

[1] Hippocampus: Distance = 1.11 [1.01], median [IQR], n = 195,681 timepoints; EC: Distance = 0.94 [1.10], median [IQR], n = 133,761 timepoints; Amygdala: Distance = 0.78 [0.88], median [IQR], n = 165,281 timepoints.

[2] Hippocampus: Distance = 0.60 [0.70], median [IQR], n = 8,772 combinations; EC: Distance = 0.28 [0.52], median [IQR], n = 5,017 combinations ($p < 0.01$; Brunner–Munzel test); Amygdala: Distance = 0.24 [0.42], median [IQR], n = 7,466 combinations ($p < 0.01$; Brunner–Munzel test).

3.3. Memory load-dependent neural trajectory distance between encoding and retrieval states in the hippocampus

In terms of memory load in the Stenberg task, we identified a negative correlation between the correct rate of trials and set size (the number of letters to encode) (Figure 3A).[3] Similarly, a positive correlation was observed between the response time and set size (Figure 3B).[4].

Furthermore, we found a positive correlation between set size and the trajectory distance between the encoding and retrieval phases ($\log_{10}\|g_E g_R\|$) (Figure 3C).[5]. However, distances between other combinations of phases did not display statistically significant correlations (Figures 3D and S2).

3.4. Detection of hippocampal SWR from putative CA1 regions

For precision improvement in recording sites and SWR detection, we estimated the electrode placements in the CA1 regions of the hippocampus using distinct multiunit spike patterns during the SWR events. SWR^+/SWR^- candidates from every session and hippocampal region were embedded in a two-dimensional space using UMAP (Figure 4A).[6] We used the silhouette score as a metric for quality of clustering (Figure 4B and Table 2). Recording sites with an average silhouette score exceeding 0.6 across all sessions were identified as putative CA1 regions.[7] (Tables 2 and 3). We identified five putative CA1 regions, four of which were not labeled as seizure onset zones (Table 1).

Subsequently, SWR^+/SWR^- candidates within these putative CA1 regions were labeled as SWR^+ and SWR^-, respectively[8] (Table 3). Both SWR^+ and SWR^- exhibited the same duration[9] (Figure 4C) due to their definitions, and followed a log-distribution. We observed an augmentation in SWR^+ incidence during the initial 400 ms of the retrieval phase[10] (Figure 4D). The peak ripple band amplitude of SWR^+ outpaced SWR^- and followed a log-normal distribution (Figure 4E).[11].

3.5. Transient changes in hippocampal neural trajectory during SWR

We computed the distance of the trajectory from the origin (O) during SWR events in both the encoding and retrieval phases (Figure 5A). Observing the increase in distance during SWR as shown in Figure 5A, we differentiated each SWR into three stages: pre-, mid-, and post-SWR. Therefore, the distances from O during those SWR periods are identified as $\|\text{pre-eSWR}^+\|$, $\|\text{mid-eSWR}^+\|$ among others.

$\|\text{mid-eSWR}^+\|$[12] was greater than $\|\text{pre-eSWR}^+\|$[13], and $\|\text{mid-rSWR}^+\|$[14] was larger than $\|\text{pre-rSWR}^+\|$ in both Match IN and Mismatch OUT tasks.[15].

3.6. Visualization of hippocampal neural trajectory during SWR in two-dimensional spaces

Following our observations of neural trajectory 'jumping' during SWR (Figure 5), we visualized the three-dimensional trajectories of pre-, mid-, and post-SWR events during the encoding and retrieval phases (Figure 6), the distance between which was found to be

[3]Correct rate: set size four (0.99 ±0.11, mean ±SD; n = 333 trials) vs. set size six (0.93 ±0.26; n = 278 trials; $p < 0.001$, Brunner–Munzel test with Bonferroni correction) and set size eight (0.87 ±0.34; n = 275 trials; $p < 0.05$; Brunner–Munzel test with Bonferroni correction). Overall, $p < 0.001$ for Kruskal–Wallis test; correlation coefficient = -0.20, $p < 0.001$.

[4]Response time: set size four (1.26 ±0.45 s; n = 333 trials) vs. set size six (1.53 ±0.91 s; n = 278 trials) and set size eight (1.66 ±0.80 s; n = 275 trials). All comparisons $p < 0.001$, Brunner–Munzel test with Bonferroni correction; $p < 0.001$ for Kruskal–Wallis test; correlation coefficient = 0.22, $p < 0.001$

[5]Correlation between set size and $\log_{10}(\|g_E g_R\|)$: correlation coefficient = 0.05, $p < 0.001$. Specific values: $\|g_E g_R\|$ = 0.54 [0.70] for set size four, n = 447; $\|g_E g_R\|$ = 0.58 [0.66] for set size six, n = 381; $\|g_E g_R\|$ = 0.61 [0.63] for set size eight, n = 395.

[6]Consider the AHL in session #1 of subject #1, for illustration purposes.

[7]The identified regions were: AHL of subject #1, AHR of subject #3, PHL of subject #4, AHL of subject #6, and AHR of subject #9.

[8]These definitions led to equal counts for both categories: SWR^+ (n = 1,170) and SWR^- (n = 1,170).

[9]These definitions led to equal durations for both categories: SWR^+ (93.0 [65.4] ms) and SWR^- (93.0 [65.4] ms).

[10]SWR^+ increased against the bootstrap sample; 95th percentile = 0.42 [Hz]; $p < 0.05$.

[11]SWR^+ (3.05 [0.85] SD of baseline, median [IQR]; n = 1,170) vs. SWR^- (2.37 [0.33] SD of baseline, median [IQR]; n = 1,170; $p < 0.001$; Brunner–Munzel test).

[12]1.25 [1.30], median [IQR], n = 1,281, in Match IN task; 1.12 [1.35], median [IQR], n = 1,163, in Mismatch OUT task

[13]1.08 [1.07], median [IQR], n = 1,149, in Match IN task; 0.90 [1.12], median [IQR], n = 1,088, in Mismatch OUT task

[14]1.32 [1.24], median [IQR], n = 935, in Match IN task; 1.15 [1.26], median [IQR], n = 891, in Mismatch OUT task

[15]1.19 [0.96], median [IQR], n = 673, in Match IN task; 0.94 [0.88], median [IQR], n = 664, in Mismatch OUT task

memory-load dependent (Figure 3).

To provide two-dimensional visualization, we linearly aligned peri-SWR trajectories by assigning g_E at the origin (0, 0) and g_R at ($\|g_E g_R\|$, 0). Post this, we rotated these aligned trajectories around the $g_E g_R$ axis (the x-axis). Thus, the distances from the origin in the original three-dimensional spaces are preserved in the two-dimensional equivalent.

The scatter plot within these two-dimensional spaces reveals characteristic distributions of peri-SWR trajectories based on phases and task types. For instance, one can observe that the magnitude of $\|\text{mid-eSWR}^+\|$ surpasses that of $\|\text{pre-eSWR}^+\|$ (Figure 6B), consistent with our earlier findings (Figure 5).

3.7. Fluctuations of hippocampal neural trajectories between encoding and retrieval states

Next, we examined trajectory *directions* in relation to $\overrightarrow{g_E g_R}$. The directions of SWRs were defined by the neural trajectory at −250 ms and +250 ms from their center, i.e., $\overrightarrow{\text{eSWR}^+}$.

We calculated the density of $\overrightarrow{\text{eSWR}} \cdot \overrightarrow{g_E g_R}$, $\overrightarrow{\text{rSWR}} \cdot \overrightarrow{g_E g_R}$, and $\overrightarrow{\text{eSWR}} \cdot \overrightarrow{\text{rSWR}}$ (Figures 7A–D). $\overrightarrow{\text{rSWR}^-} \cdot \overrightarrow{g_E g_R}$ displayed a biphasic distribution.

By taking the difference between the distribution of $\overrightarrow{\text{rSWR}^+} \cdot \overrightarrow{g_E g_R}$ (Figures 7A and B) and that of $\overrightarrow{\text{rSWR}^-} \cdot \overrightarrow{g_E g_R}$ (Figures 7C and D), we computed the contributions of SWR (Figures 7E and F), which revealed a shift in the direction of $\overrightarrow{g_E g_R}$ (Figures 7E and F: *red rectangles*).

Moreover, exclusively in the Mismatch OUT task, $\overrightarrow{\text{eSWR}^+} \cdot \overrightarrow{\text{rSWR}^+}$ was less than $\overrightarrow{\text{eSWR}^-} \cdot \overrightarrow{\text{rSWR}^-}$ (baseline periods) (Figure 7F: *pink circles*). In simpler terms, eSWR and rSWR pointed in the opposite direction only in the Mismatch OUT task but not in the Match IN task (Figure 7E: *pink circles*).

4. Discussion

5. Discussion

This study hypothesized that within low-dimensional spaces during a working memory (WM) task in humans, hippocampal neurons form unique trajectories, particularly during sharp-wave ripple (SWR) periods. Initially, the multiunit spikes in medial temporal lobe (MTL) regions were projected onto three-dimensional spaces during a Sternberg task using Gaussian Process Factor Analysis (GPFA) (Figure 1D–E and Figure 2A). The distance of the trajectory across WM phases ($\|g_F g_E\|$, $\|g_F g_M\|$, $\|g_F g_R\|$, $\|g_E g_M\|$, $\|g_E g_R\|$, and $\|g_M g_R\|$) was notably larger in the hippocampus than in the EC and amygdala (Figure 2E), indicating dynamic neural activity in the hippocampus during the WM task. Further, in the hippocampus, the trajectory distance between the encoding and retrieval phases ($\|g_F g_E\|$) exhibited a positive correlation with memory load (Figure 3C–D), reflecting WM processing. The hippocampal neural trajectory was found to increase transiently during SWRs (Figure 5). Finally, the hippocampal neural trajectory switched between encoding and retrieval states, moving from encoding to retrieval during SWR events (Figure 7). These findings not only explain various facets of hippocampal neural activity during a WM task in humans but also offer new insights into how SWRs influence the switch in neural states.

We found that the distance of the neural trajectory across the phases was greater in the hippocampus compared to that in the EC and amygdala, even when considering the distance from O in these regions (Figure 2C–E). This supports the involvement of the hippocampus in the WM task, aligning with previous reports of hippocampal persistent firing during the maintenance phase [3] [4] [5] [6]. However, when we applied GPFA to multiunit activity during a 1-second level resolution of the WM task, we observed that the neural trajectory in low-dimensional space showed a memory-load dependency between the encoding and retrieval phases, symbolized as $\|g_E g_R\|$ (Figure 3). These findings corroborate the association of the hippocampus with WM processing.

Our analysis was confined to putative CA1 regions (Figure 4), which was bolstered by several factors. This specific focus stems from established observations that SWRs synchronize with spike bursts of interneurons and pyramidal neurons [44] [45] [46] [47], potentially within a 50 μm radius of the recording site [48]. We further identified an increased incidence of SWRs during the first 0–400 ms of the retrieval phase (Figure 4D). This finding harmonizes with previous reports of heightened SWR occurrence preceding spontaneous verbal recall [21] [22], supporting our results under a triggered retrieval condition. The observed log-normal distributions of both SWR duration and ripple band peak ampli-

tude in this study (Figure 4C & E) is in accordance with the consensus in this field [39]. As a result, our decision to restrict recording sites to putative CA1 regions likely contributed to enhancing the accuracy of SWR detection. However, the increase in trajectory distance from *O* during SWRs (Figure 5) might have been skewed towards higher values due to channel selection. However, this potential bias does not substantially challenge our primary findings.

Interestingly, during the retrieval phase, the trajectory directions oscillated between encoding and retrieval states during both baseline and SWR periods (Figure 7C & D). Moreover, the balance of this oscillation shifted from encoding to retrieval state during SWR events (Figure 7 E & F). These results are consistent with previous reports on the role of SWR in memory retrieval [21] [22]. Our findings highlight a new understanding, suggesting that SWRs occur when the hippocampal representation transitions from encoding to retrieval states. Therefore, these results reveal novel aspects of hippocampal representations, including (i) neuronal oscillation between encoding and retrieval states during a WM task and (ii) SWR serving as a trigger for changing neural states.

Furthermore, our study uncovered WM-task type-specific differences between encoding- and retrieval-SWRs (Figure 7E–F). Notably, opposing movements of encoding-SWR (eSWR) and retrieval-SWR (rSWR) were not observed in the Match IN task but were apparent in the Mismatch OUT task. These observations can be explained by the memory engram theory [49]. Particularly, the Match In task provided participants with previously presented letters, contrastingly, the Mismatch OUT task introduced a new letter not present in the encoding phase. These interpretations underscore the significant role of SWR in human cognitive processes.

In conclusion, the present investigation demonstrated that hippocampal activity oscillates between encoding and retrieval states during a WM task and uniquely transitions from encoding to retrieval during SWR incidents. These findings provide meaningful insight into the neural counterparts and functionality of working memory in the hippocampus.

References

[1] W. B. Scoville, B. Milner, LOSS OF RECENT MEMORY AFTER BILATERAL HIPPOCAMPAL LESIONS, Journal of Neurology, Neurosurgery, and Psychiatry 20 (1) (1957) 11–21. URL https://www.ncbi.nlm.nih.gov/pmc/articles/PMC497229/

[2] L. R. Squire, The Legacy of Patient H.M. for Neuroscience, Neuron 61 (1) (2009) 6–9. doi:10.1016/j.neuron.2008.12.023.
URL https://www.ncbi.nlm.nih.gov/pmc/articles/PMC2649674/

[3] E. Boran, T. Fedele, P. Klaver, P. Hilfiker, L. Stieglitz, T. Grunwald, J. Sarnthein, Persistent hippocampal neural firing and hippocampal-cortical coupling predict verbal working memory load, Science Advances 5 (3) (2019) eaav3687. doi:10.1126/sciadv.aav3687.
URL https://www.science.org/doi/10.1126/sciadv.aav3687

[4] J. Kamiński, S. Sullivan, J. M. Chung, I. B. Ross, A. N. Mamelak, U. Rutishauser, Persistently active neurons in human medial frontal and medial temporal lobe support working memory, Nature Neuroscience 20 (4) (2017) 590–601, number: 4 Publisher: Nature Publishing Group. doi:10.1038/nn.4509.
URL https://www.nature.com/articles/nn.4509

[5] S. Kornblith, R. Q. Quiroga, C. Koch, I. Fried, F. Mormann, Persistent Single-Neuron Activity during Working Memory in the Human Medial Temporal Lobe, Current Biology 27 (7) (2017) 1026–1032, publisher: Elsevier. doi:10.1016/j.cub.2017.02.013.
URL https://www.cell.com/current-biology/abstract/S0960-9822(17)30149-5

[6] M. C. M. Faraut, A. A. Carlson, S. Sullivan, O. Tudusciuc, I. Ross, C. M. Reed, J. M. Chung, A. N. Mamelak, U. Rutishauser, Dataset of human medial temporal lobe single neuron activity during declarative memory encoding and recognition, Scientific Data 5 (1) (2018) 180010, number: 1 Publisher: Nature Publishing Group. doi:10.1038/sdata.2018.10.
URL https://www.nature.com/articles/sdata201810

[7] A. A. Borders, C. Ranganath, A. P. Yonelinas, The hippocampus supports high-precision binding in visual working memory, Hippocampus 32 (3) (2022) 217–230. doi:10.1002/hipo.23401.

[8] J. Li, D. Cao, S. Yu, X. Xiao, L. Imbach, L. Stieglitz, J. Sarnthein, T. Jiang, Functional specialization and interaction in the amygdala-hippocampus circuit during working memory processing, Nature Communications 14 (1) (2023) 2921, number: 1 Publisher: Nature Publishing Group. doi:10.1038/s41467-023-38571-w.
URL https://www.nature.com/articles/s41467-023-38571-w

[9] V. Dimakopoulos, P. Mégevand, L. H. Stieglitz, L. Imbach, J. Sarnthein, Information flows from hippocampus to auditory cortex during replay of verbal working memory items, eLife 11 (2022) e78677, publisher: eLife Sciences Publications, Ltd. doi:10.7554/eLife.78677.
URL https://doi.org/10.7554/eLife.78677

[10] G. Buzsáki, Hippocampal sharp wave-ripple: A cognitive biomarker for episodic memory and planning, Hippocampus 25 (10) (2015) 1073–1188, _eprint: https://onlinelibrary.wiley.com/doi/pdf/10.1002/hipo.22488. doi:https://doi.org/10.1002/hipo.22488.

URL https://onlinelibrary.wiley.com/doi/abs/10.1002/hipo.22488

[11] M. A. Wilson, B. L. McNaughton, Reactivation of hippocampal ensemble memories during sleep, Science (New York, N.Y.) 265 (5172) (1994) 676–679. doi:10.1126/science.8036517.

[12] Z. Nádasdy, H. Hirase, A. Czurkó, J. Csicsvari, G. Buzsáki, Replay and Time Compression of Recurring Spike Sequences in the Hippocampus, Journal of Neuroscience 19 (21) (1999) 9497–9507, publisher: Society for Neuroscience Section: ARTICLE. doi:10.1523/JNEUROSCI.19-21-09497.1999.
URL https://www.jneurosci.org/content/19/21/9497

[13] A. K. Lee, M. A. Wilson, Memory of sequential experience in the hippocampus during slow wave sleep, Neuron 36 (6) (2002) 1183–1194. doi:10.1016/s0896-6273(02)01096-6.

[14] K. Diba, G. Buzsáki, Forward and reverse hippocampal place-cell sequences during ripples, Nature Neuroscience 10 (10) (2007) 1241–1242, number: 10 Publisher: Nature Publishing Group. doi:10.1038/nn1961.
URL https://www.nature.com/articles/nn1961

[15] T. J. Davidson, F. Kloosterman, M. A. Wilson, Hippocampal replay of extended experience, Neuron 63 (4) (2009) 497–507. doi:10.1016/j.neuron.2009.07.027.

[16] G. Girardeau, K. Benchenane, S. I. Wiener, G. Buzsáki, M. B. Zugaro, Selective suppression of hippocampal ripples impairs spatial memory, Nature Neuroscience 12 (10) (2009) 1222–1223. doi:10.1038/nn.2384.
URL http://www.nature.com/articles/nn.2384

[17] V. Ego-Stengel, M. A. Wilson, Disruption of ripple-associated hippocampal activity during rest impairs spatial learning in the rat, Hippocampus 20 (1) (2010) 1–10. doi:10.1002/hipo.20707.

[18] A. Fernández-Ruiz, A. Oliva, E. Fermino de Oliveira, F. Rocha-Almeida, D. Tingley, G. Buzsáki, Long-duration hippocampal sharp wave ripples improve memory, Science (New York, N.Y.) 364 (6445) (2019) 1082–1086. doi:10.1126/science.aax0758.
URL https://www.ncbi.nlm.nih.gov/pmc/articles/PMC6693581/

[19] J. Kim, A. Joshi, L. Frank, K. Ganguly, Cortical–hippocampal coupling during manifold exploration in motor cortex, Nature (2022) 1–8Publisher: Nature Publishing Group. doi:10.1038/s41586-022-05533-z.
URL https://www.nature.com/articles/s41586-022-05533-z

[20] C.-T. Wu, D. Haggerty, C. Kemere, D. Ji, Hippocampal awake replay in fear memory retrieval, Nature Neuroscience 20 (4) (2017) 571–580. doi:10.1038/nn.4507.

[21] Y. Norman, E. M. Yeagle, S. Khuvis, M. Harel, A. D. Mehta, R. Malach, Hippocampal sharp-wave ripples linked to visual episodic recollection in humans, Science 365 (6454) (2019) eaax1030. doi:10.1126/science.aax1030.
URL https://www.sciencemag.org/lookup/doi/10.1126/science.aax1030

[22] Y. Norman, O. Raccah, S. Liu, J. Parvizi, R. Malach, Hippocampal ripples and their coordinated dialogue with the default mode network during recent and remote recollection, Neuron 109 (17) (2021) 2767–2780.e5, publisher: Elsevier. doi:10.1016/j.neuron.2021.06.020.
URL https://www.cell.com/neuron/abstract/S0896-6273(21)00461-X

[23] C. J. Behrens, L. P. van den Boom, L. de Hoz, A. Friedman, U. Heinemann, Induction of sharp wave–ripple complexes in vitro and reorganization of hippocampal networks, Nature Neuroscience 8 (11) (2005) 1560–1567, number: 11 Publisher: Nature Publishing Group. doi:10.1038/nn1571.
URL https://www.nature.com/articles/nn1571

[24] H. Norimoto, K. Makino, M. Gao, Y. Shikano, K. Okamoto, T. Ishikawa, T. Sasaki, H. Hioki, S. Fujisawa, Y. Ikegaya, Hippocampal ripples down-regulate synapses, Science (New York, N.Y.) 359 (6383) (2018) 1524–1527. doi:10.1126/science.aao0702.

[25] S. P. Jadhav, C. Kemere, P. W. German, L. M. Frank, Awake Hippocampal Sharp-Wave Ripples Support Spatial Memory, Science 336 (6087) (2012) 1454–1458, publisher: American Association for the Advancement of Science. doi:10.1126/science.1217230.
URL https://www.science.org/doi/abs/10.1126/science.1217230

[26] J. O'Keefe, J. Dostrovsky, The hippocampus as a spatial map: Preliminary evidence from unit activity in the freely-moving rat, Brain Research 34 (1971) 171–175, place: Netherlands Publisher: Elsevier Science. doi:10.1016/0006-8993(71)90358-1.

[27] J. O'Keefe, Place units in the hippocampus of the freely moving rat, Experimental Neurology 51 (1) (1976) 78–109. doi:10.1016/0014-4886(76)90055-8.
URL https://www.sciencedirect.com/science/article/pii/0014488676900558

[28] A. D. Ekstrom, M. J. Kahana, J. B. Caplan, T. A. Fields, E. A. Isham, E. L. Newman, I. Fried, Cellular networks underlying human spatial navigation, Nature 425 (6954) (2003) 184–188, number: 6954 Publisher: Nature Publishing Group. doi:10.1038/nature01964.
URL https://www.nature.com/articles/nature01964

[29] K. B. Kjelstrup, T. Solstad, V. H. Brun, T. Hafting, S. Leutgeb, M. P. Witter, E. I. Moser, M.-B. Moser, Finite Scale of Spatial Representation in the Hippocampus, Science 321 (5885) (2008) 140–143, publisher: American Association for the Advancement of Science. doi:10.1126/science.1157086.
URL https://www.science.org/doi/abs/10.1126/science.1157086

[30] C. D. Harvey, F. Collman, D. A. Dombeck, D. W. Tank, Intracellular dynamics of hippocampal place cells during virtual navigation, Nature 461 (7266) (2009) 941–946, number: 7266 Publisher: Nature Publishing Group. doi:10.1038/nature08499.
URL https://www.nature.com/articles/nature08499

[31] H. Zhang, P. D. Rich, A. K. Lee, T. O. Sharpee, Hippocampal spatial representations exhibit a hyperbolic geometry that expands with experience, Nature Neuroscience (Dec. 2022). doi:10.1038/s41593-022-01212-4.
URL https://www.nature.com/articles/s41593-022-01212-4

[32] P. A. Naber, F. H. Lopes da Silva, M. P. Witter, Reciprocal connections between the entorhinal cortex and hippocampal fields CA1 and the subiculum are in reg-

ister with the projections from CA1 to the subiculum, Hippocampus 11 (2) (2001) 99–104, _eprint: https://onlinelibrary.wiley.com/doi/pdf/10.1002/hipo.1028. doi:10.1002/hipo.1028.
URL https://onlinelibrary.wiley.com/doi/abs/10.1002/hipo.1028

[33] N. M. van Strien, N. L. M. Cappaert, M. P. Witter, The anatomy of memory: an interactive overview of the parahippocampal–hippocampal network, Nature Reviews Neuroscience 10 (4) (2009) 272–282, number: 4 Publisher: Nature Publishing Group. doi:10.1038/nrn2614.
URL https://www.nature.com/articles/nrn2614

[34] B. A. Strange, M. P. Witter, E. S. Lein, E. I. Moser, Functional organization of the hippocampal longitudinal axis, Nature Reviews Neuroscience 15 (10) (2014) 655–669, number: 10 Publisher: Nature Publishing Group. doi:10.1038/nrn3785.
URL https://www.nature.com/articles/nrn3785

[35] R. J. Gardner, E. Hermansen, M. Pachitariu, Y. Burak, N. A. Baas, B. A. Dunn, M.-B. Moser, E. I. Moser, Toroidal topology of population activity in grid cells, Nature 602 (7895) (2022) 123–128, number: 7895 Publisher: Nature Publishing Group. doi:10.1038/s41586-021-04268-7.
URL https://www.nature.com/articles/s41586-021-04268-7

[36] E. Boran, T. Fedele, A. Steiner, P. Hilfiker, L. Stieglitz, T. Grunwald, J. Sarnthein, Dataset of human medial temporal lobe neurons, scalp and intracranial EEG during a verbal working memory task, Scientific Data 7 (1) (2020) 30, number: 1 Publisher: Nature Publishing Group. doi:10.1038/s41597-020-0364-3.
URL https://www.nature.com/articles/s41597-020-0364-3

[37] B. M. Yu, J. P. Cunningham, G. Santhanam, S. I. Ryu, K. V. Shenoy, M. Sahani, Gaussian-Process Factor Analysis for Low-Dimensional Single-Trial Analysis of Neural Population Activity, Journal of Neurophysiology 102 (1) (2009) 614–635. doi:10.1152/jn.90941.2008.
URL https://www.ncbi.nlm.nih.gov/pmc/articles/PMC2712272/

[38] J. Niediek, J. Boström, C. E. Elger, F. Mormann, Reliable Analysis of Single-Unit Recordings from the Human Brain under Noisy Conditions: Tracking Neurons over Hours, PLOS ONE 11 (12) (2016) e0166598, publisher: Public Library of Science. doi:10.1371/journal.pone.0166598.
URL https://journals.plos.org/plosone/article?id=10.1371/journal.pone.0166598

[39] A. A. Liu, S. Henin, S. Abbaspoor, A. Bragin, E. A. Buffalo, J. S. Farrell, D. J. Foster, L. M. Frank, T. Gedankien, J. Gotman, J. A. Guidera, K. L. Hoffman, J. Jacobs, M. J. Kahana, L. Li, Z. Liao, J. J. Lin, A. Losonczy, R. Malach, M. A. van der Meer, K. McClain, B. L. McNaughton, Y. Norman, A. Navas-Olive, L. M. de la Prida, J. W. Rueckemann, J. J. Sakon, I. Skelin, I. Soltesz, B. P. Staresina, S. A. Weiss, M. A. Wilson, K. A. Zaghloul, M. Zugaro, G. Buzsáki, A consensus statement on detection of hippocampal sharp wave ripples and differentiation from other fast oscillations, Nature Communications 13 (1) (2022) 6000, number: 1 Publisher: Nature Publishing Group. doi:10.1038/s41467-022-33536-x.
URL https://www.nature.com/articles/s41467-022-33536-x

[40] K. Kay, M. Sosa, J. E. Chung, M. P. Karlsson, M. C. Larkin, L. M. Frank, A hippocampal network for spatial coding during immobility and sleep, Nature 531 (7593) (2016) 185–190. doi:10.1038/nature17144.

[41] L. McInnes, J. Healy, N. Saul, L. Großberger, UMAP: Uniform Manifold Approximation and Projection, Journal of Open Source Software 3 (29) (2018) 861. doi:10.21105/joss.00861.
URL https://joss.theoj.org/papers/10.21105/joss.00861

[42] P. J. Rousseeuw, Silhouettes: A graphical aid to the interpretation and validation of cluster analysis, Journal of Computational and Applied Mathematics 20 (1987) 53–65. doi:10.1016/0377-0427(87)90125-7.
URL https://www.sciencedirect.com/science/article/pii/0377042787901257

[43] P. Virtanen, R. Gommers, T. E. Oliphant, M. Haberland, T. Reddy, D. Cournapeau, E. Burovski, P. Peterson, W. Weckesser, J. Bright, S. J. van der Walt, M. Brett, J. Wilson, K. J. Millman, N. Mayorov, A. R. J. Nelson, E. Jones, R. Kern, E. Larson, C. J. Carey, Polat, Y. Feng, E. W. Moore, J. VanderPlas, D. Laxalde, J. Perktold, R. Cimrman, I. Henriksen, E. A. Quintero, C. R. Harris, A. M. Archibald, A. H. Ribeiro, F. Pedregosa, P. van Mulbregt, SciPy 1. 0 Contributors, SciPy 1.0: fundamental algorithms for scientific computing in Python, Nature Methods 17 (2020) 261–272, aDS Bibcode: 2020NatMe..17..261V. doi:10.1038/s41592-019-0686-2.
URL https://ui.adsabs.harvard.edu/abs/2020NatMe..17..261V

[44] G. Buzsáki, Two-stage model of memory trace formation: a role for "noisy" brain states, Neuroscience 31 (3) (1989) 551–570. doi:10.1016/0306-4522(89)90423-5.

[45] M. L. V. Quyen, A. Bragin, R. Staba, B. Crépon, C. L. Wilson, J. Engel, Cell Type-Specific Firing during Ripple Oscillations in the Hippocampal Formation of Humans, Journal of Neuroscience 28 (24) (2008) 6104–6110, publisher: Society for Neuroscience Section: Brief Communications. doi:10.1523/JNEUROSCI.0437-08.2008.
URL https://www.jneurosci.org/content/28/24/6104

[46] S. Royer, B. V. Zemelman, A. Losonczy, J. Kim, F. Chance, J. C. Magee, G. Buzsáki, Control of timing, rate and bursts of hippocampal place cells by dendritic and somatic inhibition, Nature Neuroscience 15 (5) (2012) 769–775, number: 5 Publisher: Nature Publishing Group. doi:10.1038/nn.3077.
URL https://www.nature.com/articles/nn.3077

[47] N. Hájos, M. R. Karlócai, B. Németh, I. Ulbert, H. Monyer, G. Szabó, F. Erdélyi, T. F. Freund, A. I. Gulyás, Input-output features of anatomically identified CA3 neurons during hippocampal sharp wave/ripple oscillation in vitro, The Journal of Neuroscience: The Official Journal of the Society for Neuroscience 33 (28) (2013) 11677–11691. doi:10.1523/JNEUROSCI.5729-12.2013.

[48] E. W. Schomburg, C. A. Anastassiou, G. Buzsáki, C. Koch, The Spiking Component of Oscillatory Extracellular Potentials in the Rat Hippocampus, The Journal of Neuroscience 32 (34) (2012) 11798–11811. doi:10.1523/JNEUROSCI.0656-12.2012.

URL https://www.ncbi.nlm.nih.gov/pmc/articles/PMC3459239/

[49] X. Liu, S. Ramirez, P. T. Pang, C. B. Puryear, A. Govindarajan, K. Deisseroth, S. Tonegawa, Optogenetic stimulation of a hippocampal engram activates fear memory recall, Nature 484 (7394) (2012) 381–385, number: 7394 Publisher: Nature Publishing Group. doi:10.1038/nature11028.
URL https://www.nature.com/articles/nature11028

[50] M. K. van Vugt, A. Schulze-Bonhage, B. Litt, A. Brandt, M. J. Kahana, Hippocampal Gamma Oscillations Increase with Memory Load, The Journal of Neuroscience 30 (7) (2010) 2694–2699. doi:10.1523/JNEUROSCI.0567-09.2010.
URL https://www.ncbi.nlm.nih.gov/pmc/articles/PMC2835496/

[51] K. Nader, Memory traces unbound, Trends in Neurosciences 26 (2) (2003) 65–72. doi:10.1016/S0166-2236(02)00042-5.
URL https://www.sciencedirect.com/science/article/pii/S0166223602000425

Contributors

Y.W. and T.Y. conceptualized the study; Y.W. performed the data analysis; Y.W. and T.Y. wrote the original draft; and all authors reviewed the final manuscript.

Acknowledgments

This research was funded by a grant from the Exploratory Research for Advanced Technology (JPMJER1801).

Declaration of Interests

The authors declare that they have no competing interests.

Data and code availability

The data is available on G-Node (https://doi.gin.g-node.org/10.12751/g-node.d76994/).
The source code is available on GitHub (https://github.com/yanagisawa-lab/hippocampal-neural-fluctuation-during-a-WM-task-in-humans).

Inclusion and Diversity Statement

We support inclusive, diverse, and equitable conduct of research.

Declaration of Generative AI in Scientific Writing

The authors employed ChatGPT, provided by OpenAI, for enhancing the manuscript's English language quality. After incorporating the suggested improvements, the authors meticulously revised the content. Ultimate responsibility for the final content of this publication rests entirely with the authors.

Tables

Subject ID	of sessions	AHL	AHR	PHL	PHR	ECL	ECR	AL	AR	SOZ
1	4	o	x	o	o	o	x	o	x	"AHR, LR"
2	7	o	o	o	o	o	o	o	o	"AHR, PHR"
3	3	o	o	o	o	o	o	o	x	"AHL, PHL"
4	2	o	o	o	o	o	o	o	o	"AHL, AHR, PHL, PHR"
5	3	o	x	x	o	x	x	o	x	DRR
6	6	o	o	o	o	o	o	o	o	"AHL, PHL, ECL, AL"
7	4	o	o	o	o	o	o	o	o	"AHR, PHR"
8	5	o	o	o	o	o	o	o	o	ECR
9	2	o	o	o	o	o	o	o	o	"ECR, AR"

Table 1 – Distribution of Electrodes within the Dataset

This figure represents the electrode placements and the seizure onset zones. Regions designated with "o" were available in the dataset, whereas those marked with "x" (*navy*) were not present. Abbreviations include: AHL, left hippocampal head; AHR, right hippocampal head; PHL, left hippocampal body; PHR, right hippocampal body; ECL, left entorhinal cortex; ECR, right entorhinal cortex; AL, left amygdala; AR, right amygdala; and SOZ symbolizes the seizure onset zone.

Subject	AHL	AHR	PHL	PHR
1	0.60 ± 0.14	n.a.	n.a.	0.1 ± 0
2	0.21 ± 0.16	0.17 ± 0.21	0.18 ± 0.22	0.20 ± 0.15
3	0.40 ± 0.42	0.83 ± 0.12	n.a.	n.a.
4	0.10 ± 0.00	0.10 ± 0.00	0.90 ± 0.00	0.10 ± 0.14
5	n.a.	n.a.	n.a.	n.a.
6	0.63 ± 0.06	n.a.	n.a.	0.27 ± 0.06
7	0.10 ± 0.00	0.35 ± 0.35	0.37 ± 0.47	0.10 ± 0.00
8	0.13 ± 0.10	n.a.	0.28 ± 0.49	n.a.
9	n.a.	0.85 ± 0.07	0.15 ± 0.07	n.a.

Table 2 – Silhouette score of UMAP clustering for SWR^{+} candidates and SWR^{-} candidates

The silhouette scores (mean ± SD across sessions per subject) for UMAP clustering of SWR+ candidates and SWR candidates (Figure 4A) were calculated based on their corresponding multiunit spike patterns (mean values were 0.205 [0.285], median [IQR]; Figure 4B).

Subject ID	of sessions	of trials	ROI	of SWRs	SWR incidence [Hz]
1	2	100	AHL	274	0.34
3	2	97	AHR	325	0.42
4	2	99	PHL	202	0.26
6	2	100	AHL	297	0.37
9	2	97	AHR	72	0.09
Total = 10	Total = 493	"Total = 1,170"	0.30 ± 0.13 (mean ± SD)		

Table 3 – Accounting for Defined SWR Events

The table collates statistics of putative CA1 regions and SWR events. Only the first two sessions (sessions 1 and 2) from each subject were considered to minimize sampling bias.

Figures

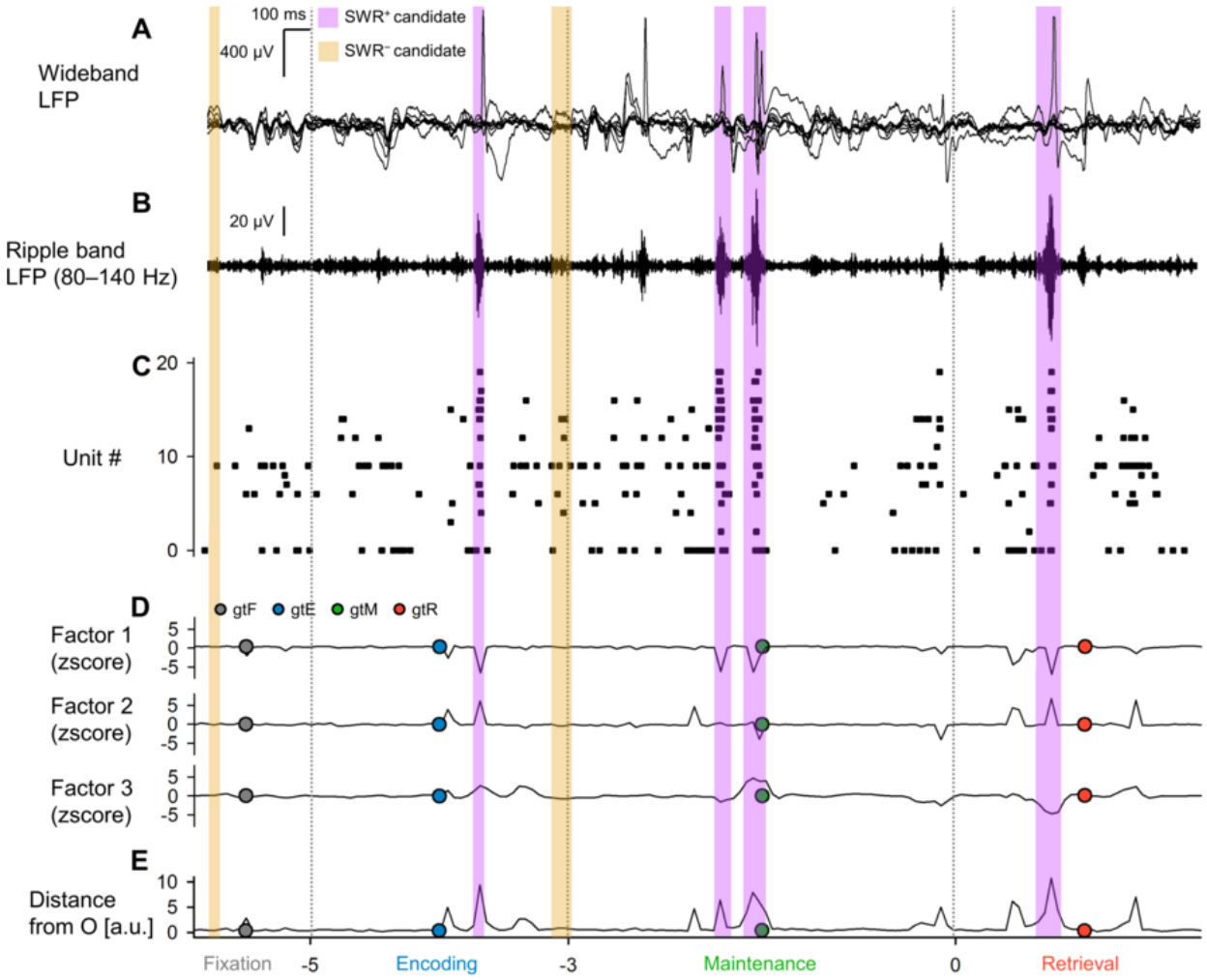

Figure 1 – ~~**Local Field Potential (LFP), Multiunit Activity, and Neural Trajectory of the Hippocampus during a Modified Sternberg Task** [8? , 9]~~ **Local Field Potentials (LFP), Multiunit Activity, and Neural Trajectories in the Hippocampus During a Modified Sternberg Task**

A. ~~This segment presents representative wideband LFP traces from iEEG signals, observed in the left hippocampal head throughout the completion of a modified Sternberg working memory task. The task involves fixation (~~These traces show representative wideband LFP intracranial EEG (iEEG) signals recorded from the left hippocampal head. The subject performed a modified Sternberg working memory task, which includes fixation (1 ~~s,~~ s, *gray*~~), encoding (~~), encoding (2 ~~s,~~ s, *blue*~~), maintenance (~~), maintenance (3 ~~s,~~ s, *green*~~), and retrieval (~~), and retrieval (2 ~~s,~~ s, *red*~~) [8? , 9].~~). ***B.*** ~~The corresponding ripple band LFP traces are depicted here [48, 23, 24].~~ We then present the corresponding ripple band LFP traces. ***C.*** ~~The raster plot of multiunit spikes, derived from the LFP traces utilizing a spike sorting algorithm, is illustrated here [38].~~ The raster plot depicts multiunit spikes taken from the LFP traces, sorted using a spike algorithm [38]. ***D.*** ~~This part represents the neural trajectory, established by the GPFA, computed from the spike counts per unit within~~ Subsequently, we illustrate the neural trajectories, which are calculated by GPFA on spike counts per unit with 50-ms ~~bins [37]. The dotted circles represent the geometric median coordinates for each phase.~~ bins. Each phase's geometric median is marked by the dot circles. ***E.*** ~~The distance from the trajectory to the point~~ The trajectory's distance from the origin *O* ~~is demonstrated here. It is notable that the~~ is portrayed, with *purple* and *yellow* ~~rectangles denote the timings for SWR~~rectangles indicating the timings for SWR$^+$ ~~candidates and SWR~~candidates and SWR$^-$ ~~candidates, respectively, functioning as controls for SWR~~candidates (considered as controls for SWR$^+$ ~~[50, 1, 40, 51, 11, 12, 13].~~), respectively.

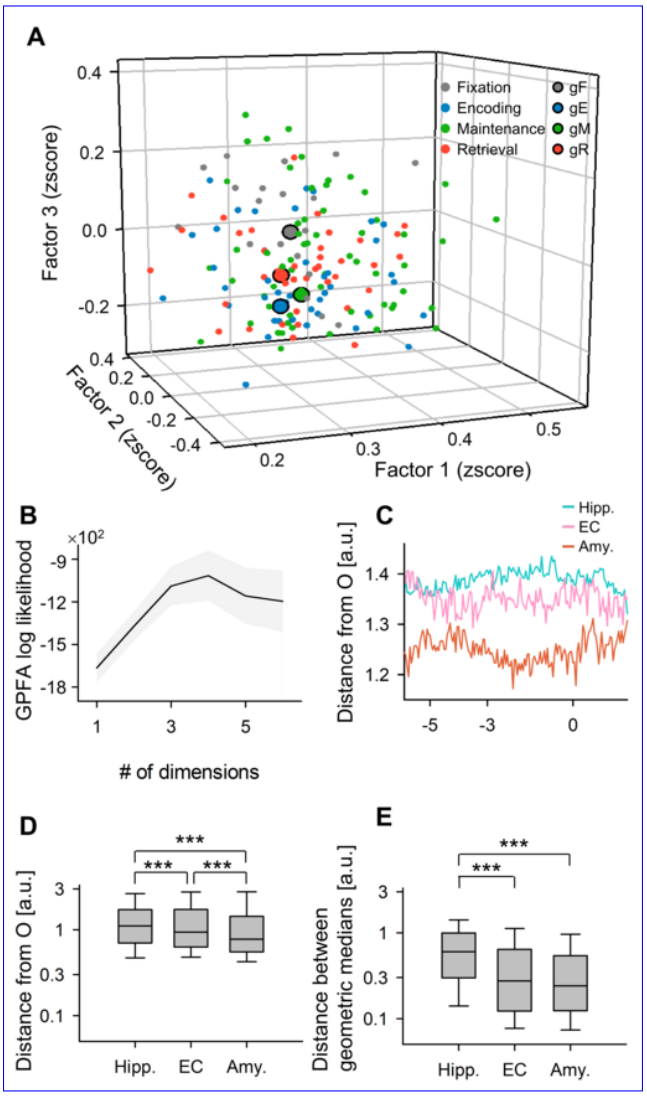

Figure 2 – ~~**State-dependent Hippocampal Neural Trajectory**~~ **State-Dependent Trajectories of Hippocampal Neurons**

A. ~~This figure presents the neural trajectory~~ Neural trajectories within the ~~first three dimensions,~~ initial three-dimensional factors derived ~~using~~ from the Gaussian Process Factor Analysis (GPFA) are displayed. ~~Each~~ The smaller ~~dot signifies the~~ dots correspond to coordinates of ~~a~~ 50-ms neural trajectory ~~bin~~bins, while the larger dots ~~indicated in~~ with *black* ~~represent~~ edges signify the geometric medians ~~of successive phases~~ for respective stages in the Sternberg working memory task~~. The phases include~~ : fixation (*gray*), encoding (*blue*), maintenance (*green*), and retrieval (*red*)~~[37]~~. ***B.*** The ~~graph shows~~ figure conveys the log-likelihood of the GPFA models ~~compared to~~ versus the ~~number~~ count of dimensions ~~employed for embedding multi-unit~~ used to embed multiunit spikes ~~within~~ found in the medial temporal lobe (MTL) ~~regions~~territories. ~~Notably~~In specific, the elbow method pinpointed the optimal ~~dimensionality was found~~ dimension to be three~~, based on the elbow method[43]~~. ***C.*** This ~~section delineates~~ panel illustrates the distance ~~between~~ of the neural ~~trajectory and~~ trajectories from the origin (*O*) for the hippocampus (Hipp.), entorhinal cortex (EC), and amygdala (Amy.), ~~and plots it over time since~~ against the ~~onset of~~ time elapsed from the probe ~~[36]~~onset. ***D.*** The ~~subsequent graph underscores~~ distance of the trajectory ~~'s distance~~ from *O* ~~across~~ within MTL regions ~~, with the~~ is displayed. The hippocampus ~~registering~~ shows the ~~most extensive~~ farthest distance, followed by the EC and the Amygdala~~[18]~~. ***E.*** The ~~final depiction signifies the~~ plot represents inter-phase trajectory distances within the MTL regions~~[39]~~. Abbreviations:

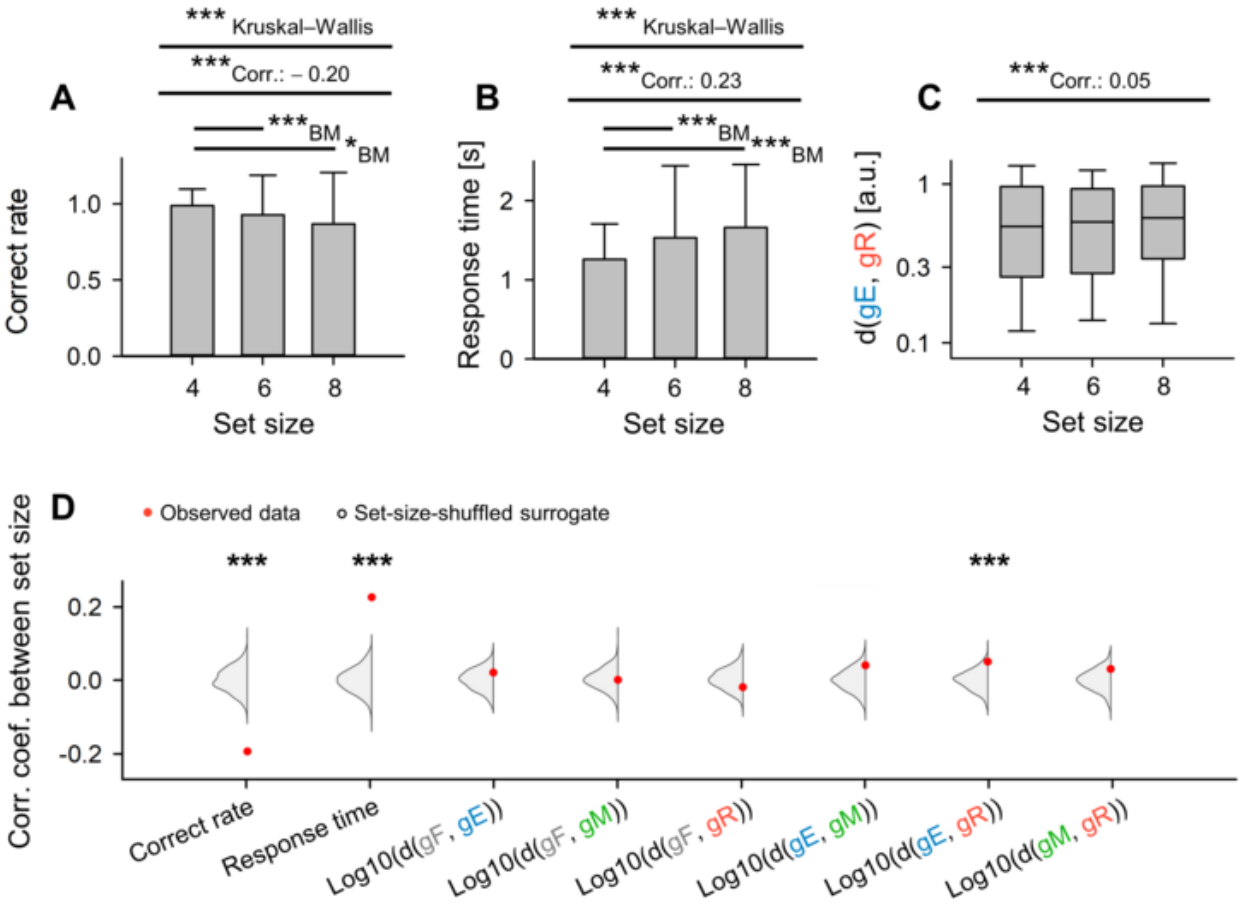

Figure 3 – ~~**Dependence of Trajectory Distance on Memory Load Between Encoding and Retrieval States in the Hippocampus**~~ **Dependency of Trajectory Distance on Memory Load: Encoding and Retrieval States in Hippocampus**

A. ~~A significant correlation has been documented~~ The relationship between ~~the~~ set size (~~the~~ number of letters that need to ~~encode~~be encoded) and ~~the correctness~~ correct rate in the ~~WM~~ working memory task (coefficient = −0.20, ***p < 0.001)~~[50, 8, 7]~~. ***B.*** ~~A notable~~ The correlation ~~exists~~ between set size and response time (coefficient = ~~0.23~~0.23, ***p < 0.001)~~[9]~~. ***C.*** ~~There is a correlation between~~ The impact of set size ~~and~~ on the inter-phase distances between the encoding and retrieval phases ($\|g_E g_R\|$/$\|g_E g_R\|$) ~~, but it's less significant~~ (correlation coefficient = 0.05)~~[8]~~. ***D.*** *Red* dots ~~express the observed~~ represent experimental observations of correlations between set size and the ~~stated~~ following parameters: correct rate, response time, ~~$\log_{10}\|g_F g_E\|$~~$\log_{10}\|g_F g_E\|$, ~~$\log_{10}\|g_F g_M\|$~~$\log_{10}\|g_F g_M\|$, ~~$\log_{10}\|g_F g_R\|$~~$\log_{10}\|g_F g_R\|$, ~~$\log_{10}\|g_E g_M\|$~~$\log_{10}\|g_E g_M\|$, ~~$\log_{10}\|g_E g_R\|$~~$\log_{10}\|g_E g_R\|$, and ~~$\log_{10}\|g_M g_R\|$~~$\log_{10}\|g_M g_R\|$. The *gray* kernel density plot illustrates the corresponding ~~randomized set-size measurements~~ set-size-shuffled surrogate (n = 1,000) (***ps < 0.001)~~[24, 47]~~.

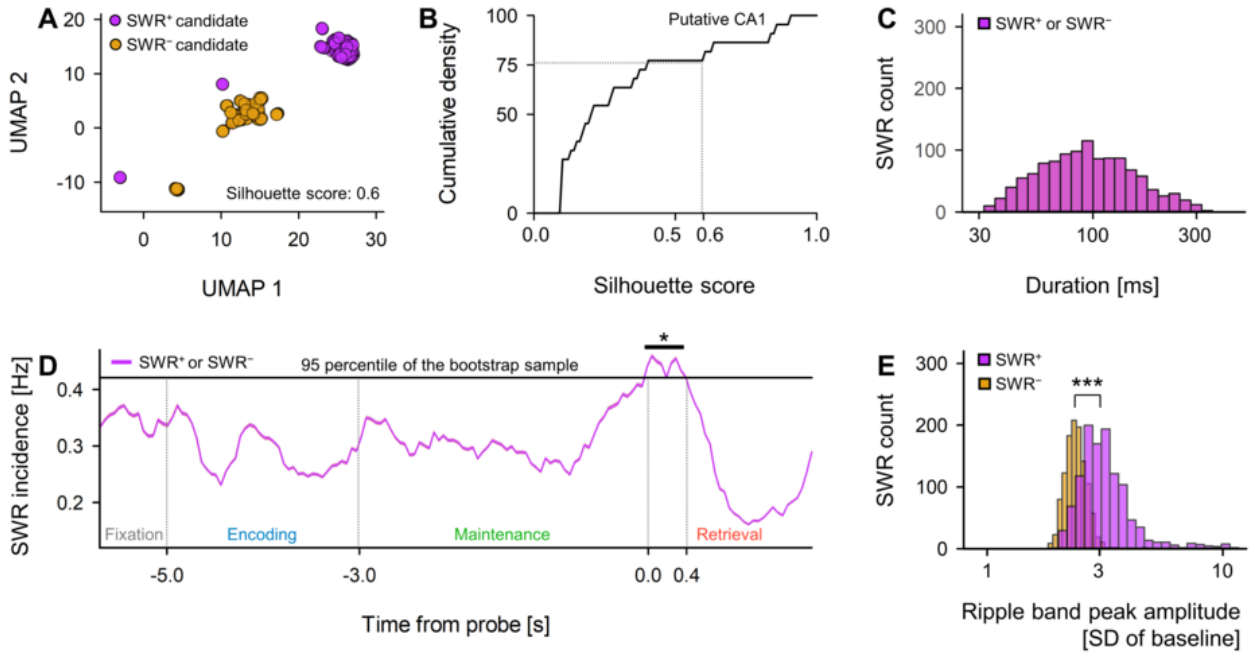

Figure 4 – ~~**Detection of SWRs in Presumed CA1 Regions**~~ **Detection of SWRs in Presumptive CA1 Regions**

A. ~~A two-dimensional~~ Two-dimensional UMAP (Uniform Manifold Approximation and Projection~~(UMAP)~~ [41] projection of ~~multi-unit~~ multiunit spikes during ~~potential SWRs~~ SWR$^+$ candidates (*purple*) and ~~non-SWRs~~ SWR$^-$ candidates (*yellow*)~~periods is given[41]~~. ***B.*** ~~The cumulative~~ Cumulative density plot ~~of~~ shows silhouette scores, ~~measuring the quality~~ indicative of UMAP clustering ~~across diverse~~ quality, for hippocampal regions ~~, is shown (refer to~~ see Table 2 for reference). ~~Regions~~ Note that ~~attained a~~ hippocampal regions with silhouette ~~score above~~ scores greater than 0.60 (~~corresponding~~ equivalent to the 75th percentile) ~~, are~~ were identified as ~~probable~~ possible CA1 ~~areas~~regions. ~~Within~~ SWR$^+$ and SWR$^-$ candidates recorded from these ~~potential~~ speculative CA1 regions ~~, the SWR and non-SWR periods~~ were respectively ~~categorized~~ classified as ~~SWRs~~ SWR$^+$ and ~~non-SWRs~~ SWR$^-$ (*ns* = 1,170)~~[42]~~. ***C.*** The identical distributions of durations are presented for ~~both SWRs~~ SWR$^+$ (*purple*) and ~~non-SWRs~~ SWR$^-$ (*yellow*)~~are depicted~~, ~~based on~~ owing to their ~~respective~~ definitions (93.0 [65.4] ms, median [IQR])~~[16][22]~~. ***D.*** ~~An illustration of the frequency of SWRs~~ SWR incidence for both SWR$^+$ (*purple*) and ~~non-SWRs~~ SWR$^-$ (*yellow*) ~~over time from~~ obtained relative to the ~~start of stimulation, represented by~~ probe's timing is illustrated as a mean ~~value~~ ±95% confidence interval~~is given~~. ~~It should~~ However, as the intervals may not be ~~noted that~~ visible due to ~~close intervals, visual differentiation can be difficult. Additionally~~their narrow range, ~~there was~~ note that a ~~discernible~~ significant increase in SWR ~~frequency~~ incidence was detected during the initial 400 ms of the retrieval phase (0.421 [Hz], *$p < 0.05$, bootstrap test)~~[10][17][18]~~. ***E.*** ~~Distributions~~ The distributions of ripple band peak amplitudes for ~~non-SWRs~~ SWR$^-$ (*yellow*; 2.37 [0.33] ~~times the standard deviation (~~SD ~~)~~ of ~~the~~ baseline, median [IQR]) and ~~SWRs~~ SWR$^+$ (*purple*; 3.05 [0.85] ~~times the~~ SD of ~~the~~ baseline, median [IQR]) are ~~exhibited. Considerable differences were observed~~ delineated (***$p < 0.001$, ~~by~~ the Brunner–Munzel test)~~[21][14][39]~~.

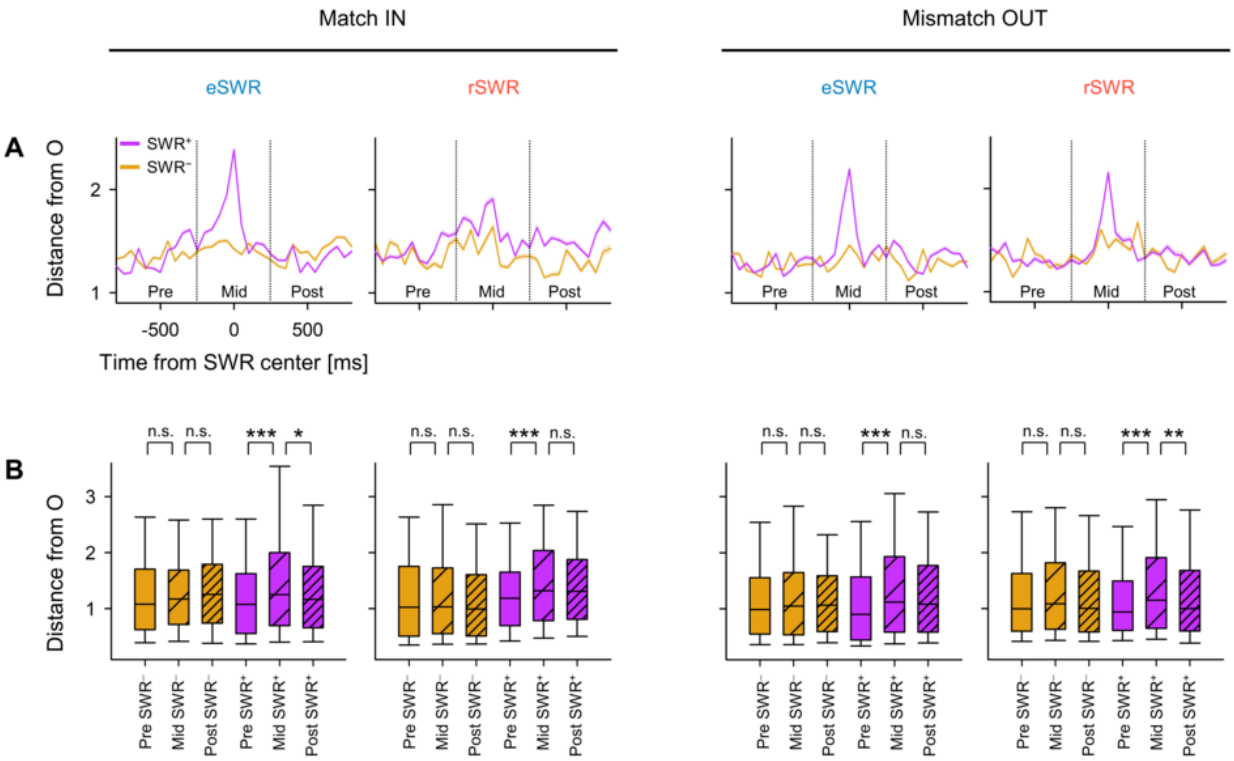

Figure 5 – ~~**Transient Changes in Neural Trajectory During SWR**~~ **Transient Alterations in Neural Trajectory During SWR Events**

A. ~~Depicts the average distance from the origin (~~Displayed is the distance from origin (*O*~~) of the ~~) of the peri-sharp-wave-ripple ~~(SWR) trajectory, alongside a~~ trajectory (mean ±95~~% confidence interval, which may not be evident due to its limited range [16, 21, 10].~~ % confidence interval). The intervals may not be apparent due to their slender ranges. ***B.*** ~~Demonstrates the distance from the origin (~~Shown is the distance from the origin (*O*~~) throughout~~) during pre-, mid-~~, and~~ , and post-SWR ~~intervals (~~periods (*$p < 0.05$, **$p < 0.01$, ***$p < 0.001$~~; according to the~~ ; assessed using the Brunner–Munzel ~~test [3]). The defined terms are: SWR,~~ test). Abbreviations: SWR, sharp-wave ~~ripple events; eSWR, SWR occurring during the encoding phase; rSWR, SWR taking place during the retrieval phase; SWR~~ripple events; eSWR, SWR during the encoding phase; rSWR, SWR while in the retrieval phase; SWR$^+$~~, an SWR event; SWR~~, positive SWR event; SWR$^-$~~, the control events aligned with SWR~~, control events for SWR$^+$; pre-, mid-~~, or~~ , or post-SWR ~~, the time segments from~~ denote the time intervals from −800 to −250 ~~ms, from~~ ms, from −250 to +250 ~~ms, and from~~ ms, or from +250 to +800 ~~ms, respectively, each relative to the SWR center.~~ ms, all relative to the center of the SWR.

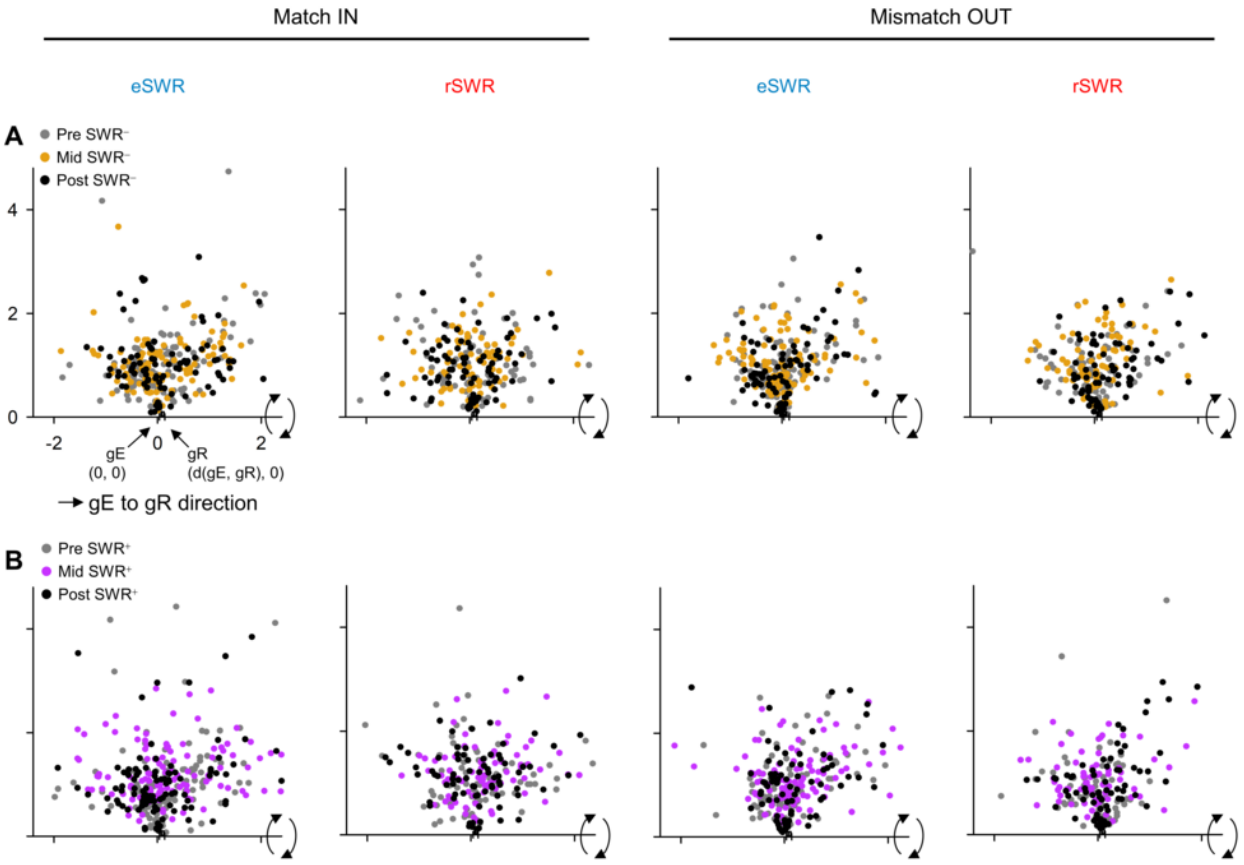

Visualization of Neural Trajectories during SWR in Two-Dimensional Spaces

~~This figure demonstrates the association of~~ The panels display hippocampal neural trajectories ~~with hippocampal activity~~ during ~~Sharp-Wave Ripple (~~SWR ~~) events in a~~ as projected onto two-dimensional ~~context~~spaces. ***A.*** ~~It depicts example~~ Indicates hippocampal neural trajectories ~~of the pre-~~ pre-SWR^{-} (*gray*), ~~mid-~~ mid-SWR^{-} (*yellow*), and post-SWR^{-} (*black*)~~phases of an SWR event [10]~~. ***B.*** ~~The trajectories that correspond with~~ Represents the equivalents for SWR^{+} ~~conditions are presented, contrasting with the~~ as opposed to SWR^{-} ~~backdrop [18]~~. ~~Variations in the magnitude of~~ The $\|g_E g_R\|$ ~~are evident across~~ varied among sessions ~~[39]~~. The projection ~~protocol is outlined as follows~~was applied in the following manner: ~~initially~~First, a linear transformation positioned g_E ~~was located~~ at the origin O (0,0), and g_R at ($\|g_E g_R\|$, 0)~~, realized through linear transformation [19]~~. ~~Subsequently, rotation of the~~ The point cloud was then rotated around the $g_E g_R$ axis (equivalent to the ~~x-axis~~x axis) ~~was conducted to accommodate a~~ for fitting into two-dimensional ~~space [37]~~spaces. ~~As a result~~Therefore, within these two-dimensional spaces, both the distances from O and the angles ~~relative to~~ preserved the original makeup of the $g_E g_R$ axis ~~remained consistent with their~~ from the original three-dimensional ~~configuration [41]~~spaces. ~~Key terms used in this context~~Abbreviations: SWR ~~pertains to Sharp-Wave Ripple~~ signifies sharp-wave ripple events; eSWR ~~means~~ denotes SWR during the encoding phase; rSWR ~~signifies~~ indicates SWR during the retrieval phase; SWR^{+} ~~defines~~ , marks an SWR event; SWR^{-} ~~represents the~~ refers to control ~~event~~ events for SWR^{+}; pre-SWR, mid-SWR, ~~and~~ or post-SWR~~indicate~~ , reference the time intervals from −800 to −250 ms, from −250 to +250 ms, ~~and~~ or from +250 to +800 ms from the center of ~~an~~ SWR~~event, respectively [31]~~.

Visualization of Neural Trajectories during SWR in Two-Dimensional Spaces

~~This figure demonstrates the association of~~ The panels display hippocampal neural trajectories ~~with hippocampal activity~~ during ~~Sharp-Wave Ripple (~~SWR ~~) events in a~~ as projected onto two-dimensional ~~context~~spaces. ***A.*** ~~It depicts example~~ Indicates hippocampal neural trajectories ~~of the pre-~~ pre-SWR^{-} (*gray*), ~~mid-~~ mid-SWR^{-} (*yellow*), and post-SWR^{-} (*black*)~~phases of an SWR event [10]~~. ***B.*** ~~The trajectories that correspond with~~ Represents the equivalents for SWR^{+} ~~conditions are presented, contrasting with the~~

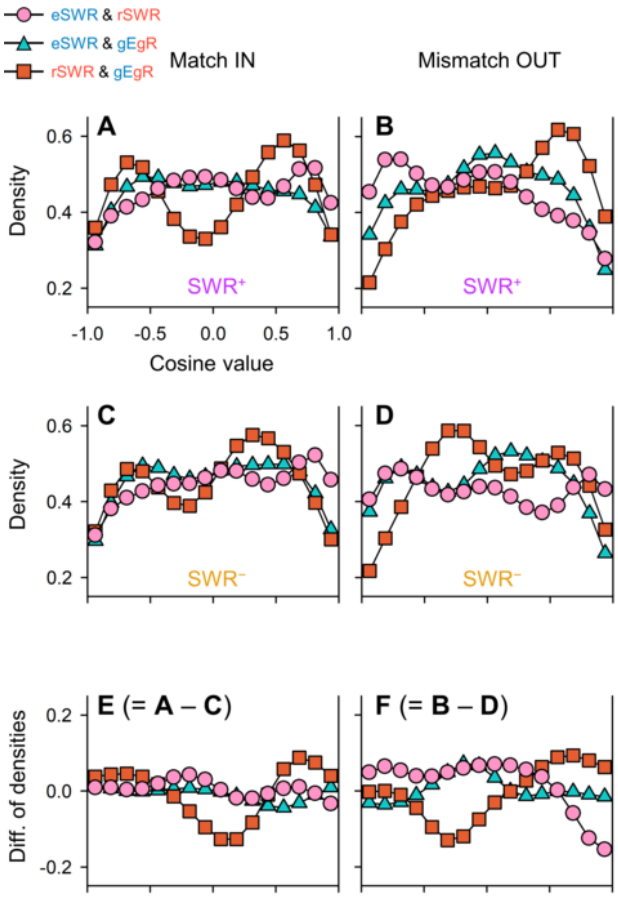

Figure 7 – ~~**Directionality of Neural Trajectories in SWR Based on Encoding and Retrieval States**~~ **Directions of Neural Trajectories during SWRs Based on Encoding and Retrieval States**

A–B ~~Depicted are the~~ Kernel ~~Density Estimation~~ density estimation (KDE) distributions of $\overrightarrow{\text{eSWR}^+} \cdot \overrightarrow{\text{rSWR}^+}$ (*pink circles*), $\overrightarrow{\text{eSWR}^+} \cdot \overrightarrow{g_E g_R}$ (*blue triangles*), and $\overrightarrow{\text{rSWR}^+} \cdot \overrightarrow{g_E g_R}$ (*red rectangles*) in Match ~~IN~~ In (*A*) and Mismatch OUT tasks (*B*) ~~[8]~~ . ***C–D*** ~~Similar~~ Present the corresponding distributions ~~for these tasks where~~ of SWR^- ~~replaces~~ instead of those of SWR^+ ~~have been presented [9]~~in *A* and *B*. ***E–F*** ~~Distinctions between~~ Depict the differences in the distributions of SWR^+ and SWR^- ~~highlight~~ , illuminating the SWR components ($E = C - A$; $F = D - B$)~~, where~~ . Note the biphasic distributions of $\overrightarrow{\text{rSWR}^-} \cdot \overrightarrow{g_E g_R}$ ~~indicate neural oscillations~~ , suggesting fluctuations between the encoding and retrieval states during the Sternberg task ~~[7]~~. ~~Contrarily~~Moreover, ~~the Mismatch OUT task showed an~~ inverse ~~relationship~~ directionality between $\overrightarrow{\text{eSWR}^+}$ and $\overrightarrow{\text{rSWR}^+}$ was observed (*pink circles*) in the Mismatch OUT task, ~~a finding~~ but not ~~observed~~ in the Match IN task ~~(~~***E–F***~~)~~ ~~[32, 33]~~. ~~Lastly~~Finally, ~~transitions~~ shifts from the retrieval to encoding ~~for~~ states were evident in the SWR components ~~were apparent~~ in both the Match IN and Mismatch OUT tasks (*red rectangles* in ~~*E–F*~~*E* and *F*) ~~[38, 48]~~.